PERGAMON

Computers and Structures 79 (2001) 1769–1779

Computers & Structures

www.elsevier.com/locate/compstruc

Performance of a macro-FEM approach using global interpolation (Coons') functions in axisymmetric potential problems

Ch. Provatidis *, A. Kanarachos

Department of Mechanical Engineering, National Technical University of Athens, 9 Heroon Polytechniou Av., Zografou Campus, GR-15773 Athens, Greece

Received 5 May 2000; accepted 28 June 2001

Abstract

This paper extends a previously presented global functional set and investigates its performance in axisymmetric potential problems. The main idea is to build-up isoparametric finite elements based on the interpolation formula developed by S.A. Coons for arbitrary-shaped CAD patches. This formula allows the global interpolation of the potential within the whole domain and leads to "large" elements, called "macro-elements". The degrees of freedom appear only at the element boundaries and can be used in the solution of both static and dynamic problems. Numerical results sustain the proposed method, which is successfully compared with conventional finite elements, boundary elements and exact analytical solutions. © 2001 Elsevier Science Ltd. All rights reserved.

Keywords: Finite elements; Macro-elements; Axisymmetric; Potential problems; Global interpolation; Coons' interpolation; Computer aided design

1. Introduction

The origin of the computational methods is rather the use of global approximation (Ritz [1], Finlayson [2], Trefftz [3]) than local approximation techniques (Argyris and Kelsey [4]). After many years of using small-size isoparametric finite elements (Zienkiewicz [5]), the development of "large" elements with the purpose of reducing mesh generation work load, the total number of degrees of freedom, as well as the computational effort in both static and dynamic regimes, has kept researchers busy for a long time. Historically, it was Irons (Irons [6]) who generalized the idea of arbitrarily noded elements, but also blending function methods based on the ideas put forward in Coons [7] have been used to produce some interesting element families (Gordon [8], Gordon and Hall [9], Zafrany and Cookson [10]).

On the other hand, large elements were introduced by schemes (Jirousek and associates [11–14]) based on Trefftz's method (Trefftz [3]). These as well as the boundary element method (BEM) (e.g. Brebbia and Dominguez [15]), require knowledge of the fundamental solution of the problem under consideration.

The Coons's interpolation method that consists the background of the proposed global interpolation method, was initially used to describe regular CAD surfaces for automotive industry (Coons [7]). This method has been generalized in a unique formula that describes C^0-, C^1-, C^2- etc. continuity of the first, second and third derivative, respectively (Kanarachos et al. [16]). In the context of the FEM, Coons's interpolation is practically used for mesh generation in structured four-sided curvilinear patches (Röper [17], Kanarachos and Röper [18], Yildir and Wexler [19]). However, as it was above

* Corresponding author. Tel.: +30-1-772-1520; fax: +30-1-772-2347.

E-mail address: prowaton@central.ntua.gr (Ch. Provatidis).

PII: S0045-7949(01)00101-8

mentioned, this interpolation can be also used to produce some interesting element families (Gordon [8]). These methods have been extended and generalized on triangles (Gordon and Hall [9], Barnhill and associates [20–22]). However, Zafrany and Cookson [10] use Coons's idea for two-dimensional problems in conjunction with Lagrange and Hermite interpolation functions, allowing a *small* number of degrees of freedom per element. Also, Zhaobei and Zhiqiang [23] apply Coons's surface method to fit boundary conditions in some families of finite element of plates and shells.

The use of large B-splines finite elements based on Coons' interpolation theory, with degrees of freedom appearing only at the element boundaries has appeared in two-dimensional potential (Kanarachos and Deriziotis [24]) and elasticity problems (Kanarachos et al. [25]). This paper extends the theory and investigates its applicability to axisymmetric potential problems, too. Numerical examples are presented for homogeneous and inhomogeneous thermal problems in structures as well as for the determination of acoustical eigenfrequencies.

2. Macro-element approach

In terms of cylindrical curvilinear coordinates r, ϑ and z (Fig. 1), fully axisymmetric potential problems, i.e. not dependent on the angular direction ϑ, include:

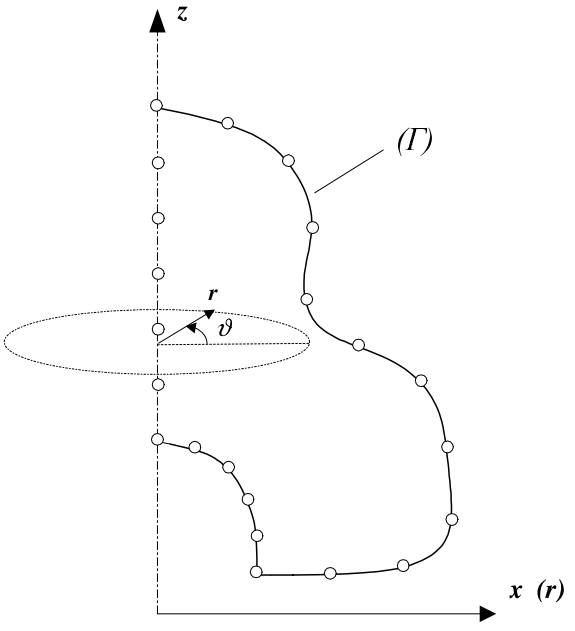

Fig. 1. Geometry definition of the general axisymmetric problem.

(i) Laplace equation

$$\nabla^2 u = \frac{\partial^2 u}{\partial r^2} + \frac{1}{r}\frac{\partial u}{\partial r} + \frac{\partial^2 u}{\partial z^2} = 0 \tag{1}$$

and also

(ii) wave propagation equation

$$\left(\frac{1}{c^2}\right)\frac{\partial^2 u}{\partial t^2} - \left(\frac{\partial^2 u}{\partial r^2} + \frac{1}{r}\frac{\partial u}{\partial r} + \frac{\partial^2 u}{\partial z^2}\right) = 0 \tag{2}$$

The boundary conditions are:

$$\begin{aligned} u &= u_\Gamma(t) \quad \text{on } \Gamma_1 \\ q &= q_\Gamma(t) \quad \text{on } \Gamma_2 \end{aligned} \tag{3}$$

In Eqs. (1)–(3) u denotes the potential, c the velocity of the wave propagation, ∇ the Nabla operator, t the time, and Γ_1 and Γ_2 parts of the boundary Γ, where the potential respectively the flux is prescribed.

As usually, analysis is performed on an axial section only and each macro-element is extended over that. In the general case, the macro-element may contain a part of the axis of symmetry and be hollow in the rest of that, as shown in Fig. 1. The x-axis is taken radially, while z-axis is taken to coincide with the axis of symmetry. The problem domain, in the (x,z) plane, is considered as a four-sided patch. This patch is mapped to a reference patch (ξ,ζ), where the normalized curvilinear coordinates vary between 0 and 1 $(0 \leqslant \xi,\zeta \leqslant 1)$ as shown in Fig. 2.

According to Coons' interpolation formula (Coons [7]), each point $\mathbf{x}(\xi,\zeta) = \{x(\xi,\zeta), z(\xi,\zeta)\}^{\mathrm{T}}$ along the patch can be approximated by its boundaries $(\mathbf{x}(\xi,0), \mathbf{x}(\xi,1), \mathbf{x}(0,\zeta), \mathbf{x}(1,\zeta))$ as follows (see also Appendix A):

$$\begin{aligned} \mathbf{x}(\xi,\zeta) = {} & E_0(\xi)\mathbf{x}(0,\zeta) + E_1(\xi)\mathbf{x}(1,\zeta) + E_0(\zeta)\mathbf{x}(\xi,0) \\ & + E_1(\zeta)\mathbf{x}(\xi,1) - E_0(\xi)E_0(\zeta)\mathbf{x}(0,0) \\ & - E_1(\xi)E_0(\zeta)\mathbf{x}(1,0) - E_0(\xi)E_1(\zeta)\mathbf{x}(0,1) \\ & - E_1(\xi)E_1(\zeta)\mathbf{x}(1,1) \end{aligned} \tag{4}$$

where for C^0-continuity discrete problems the blending functions are linear and equal to:

$$\begin{aligned} E_0(\xi) &= 1-\xi, \qquad E_1(\xi) = \xi \\ E_0(\zeta) &= 1-\zeta, \qquad E_1(\zeta) = \zeta \end{aligned} \tag{5}$$

Following the idea of isoparametric elements (Zienkiewicz [5]), Eq. (4) is extended from the geometrical quantities $\mathbf{x}(x,z)$ to the interpolation of the potential $u(\xi,\zeta)$, as follows:

$$\begin{aligned} u(\xi,\zeta) = {} & E_0(\xi)u(0,\zeta) + E_1(\xi)u(1,\zeta) + E_0(\zeta)u(\xi,0) \\ & + E_1(\zeta)u(\xi,1) - E_0(\xi)E_0(\zeta)u(0,0) \\ & - E_1(\xi)E_0(\zeta)u(1,0) - E_0(\xi)E_1(\zeta)u(0,1) \\ & - E_1(\xi)E_1(\zeta)u(1,1) \end{aligned} \tag{6}$$

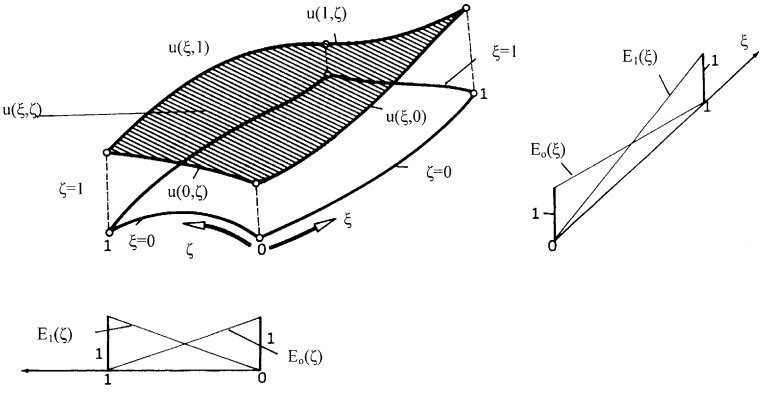

Fig. 2. Reference patch (ξ,ζ) composed of four sides ($\xi = 0$, 1 and $\zeta = 0$, 1).

If the boundary values $u(\xi,0)$, $u(\xi,1)$, $u(0,\zeta)$ and $u(1,\zeta)$ are interpolated by any set of trial functions, and then Eq. (5) is collocated to all boundary nodes, inside the reference macro-element, the solution $u(\xi,\zeta)$ is approximated by:

$$u(\xi,\zeta) = \sum_{k=1}^{N_e} N_k(\xi,\zeta)u_k(t) \tag{7}$$

with $N_k(\xi,\zeta)$ denoting the global shape functions, $u_k(t)$ nodal degrees of freedom appearing only at the boundaries of the macro-element and N_e the total number of the nodes along that.

A particular choice of trial functions is to use cubic B-splines. If now $B_j(\hat{\xi})$, where $\hat{\xi}$ is either ξ or ζ, denote cardinal splines of degree m, i.e.

$$B_j(\hat{\xi}_i) = \delta_{ij} \tag{8}$$

then the functions $u(\xi,0)$, $u(\xi,1)$, $u(0,\zeta)$ and $u(1,\zeta)$ could be written in the following form:

$$u(0,\zeta) = \sum_{j=1}^{N_q} B_j(\zeta)u(0,\zeta_j), \qquad u(1,\zeta) = \sum_{j=1}^{N_q} B_j(\zeta)u(1,\zeta_j)$$
$$u(\xi,0) = \sum_{j=1}^{N_q} B_j(\xi)u(\xi_j,0), \qquad u(\xi,1) = \sum_{j=1}^{N_q} B_j(\xi)u(\xi_j,1) \tag{9}$$

By substituting Eq. (9) into Eq. (6), the shape functions of Eq. (7) are obtained.

Typical global shape functions for a rectangular macro-element of 50 nodes are illustrated in Fig. 3. Again, these are cardinal functions ([1-0] type), exactly as in the case of conventional Lagrangian or Serendipity finite elements (Bathe [26]). For instructive purposes only, a particular application of the proposed theory to small elements is given in Appendix B.

3. Numerical implementation

Applying the well-known Galerkin procedure (Bathe [26]) to Eqs. (1) and (2), the following formulation is obtained:

$$\mathbf{M}\ddot{\mathbf{u}} + \mathbf{K}\mathbf{u} = \mathbf{f}(t) \tag{10}$$

where the mass (**M**) and stiffness (**K**) matrix are given by

$$[\mathbf{M}]_{ij} = (1/c^2)\int_\Omega N_i N_j \,\mathrm{d}\Omega = (1/c^2)\int_\Omega N_i N_j (2\pi r)\,\mathrm{d}r\,\mathrm{d}z \tag{11}$$

$$[\mathbf{K}]_{ij} = \int_\Omega \nabla N_i \nabla N_j \,\mathrm{d}\Omega = \int_\Omega \nabla N_i \nabla N_j (2\pi r)\,\mathrm{d}r\,\mathrm{d}z \tag{12}$$

and the vector of the external force (**f**) by

$$[\mathbf{f}(t)]_i = \int_\Gamma N_i \nabla u (2\pi r)\,\mathrm{d}\Gamma \tag{13}$$

The domain integrals are calculated numerically using Gaussian quadrature (e.g. 2×2 or 3×3 integration points) in cells, which are defined in the reference macro-element by $\xi =$ constant and $\zeta =$ constant families of the introduced DOFs. Obviously, the so-produced matrices $(\mathbf{M},\mathbf{K})$ are both symmetric and fully occupied.

4. Numerical results

In order to demonstrate the efficiency of the proposed macro-element approach, three model problems referring to the potential problem (1) (static case) respectively to the wave propagation problem (2) (dynamic case) with known analytical solution are presented.

In each of them, we refer to results obtained from the macro-element formulation, which are compared with conventional finite element methods (four-noded bilinear

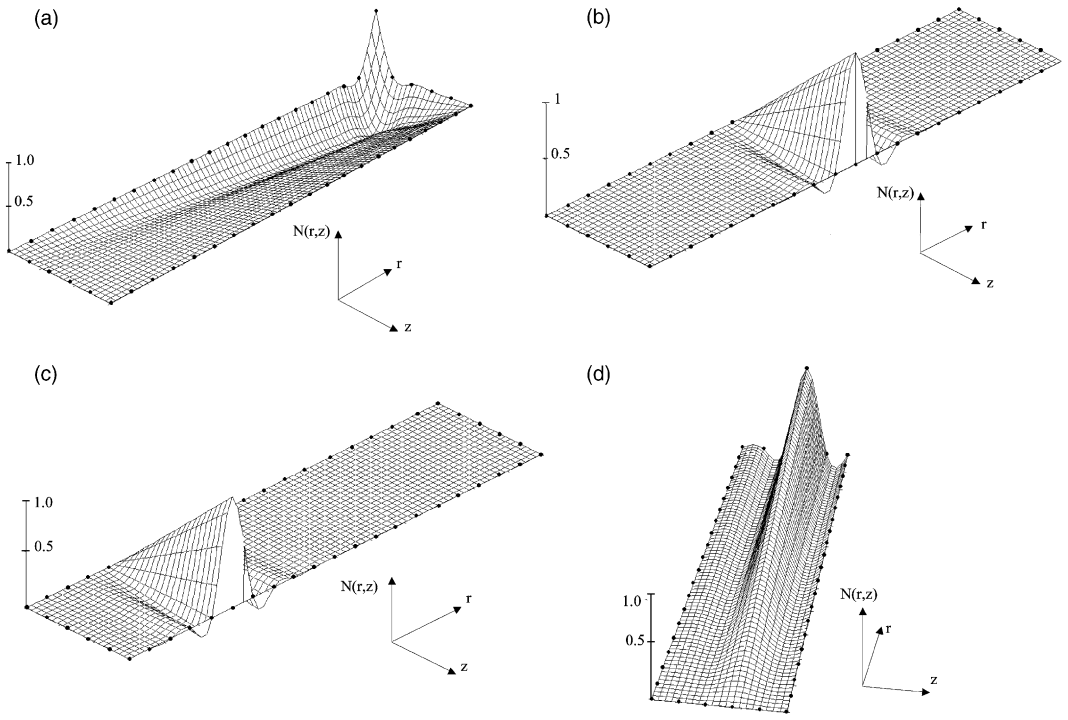

Fig. 3. Typical shape functions for a 50-noded macro-element for (a) a corner node, (b,c) nodes along the long side, and (d) along the short side.

elements) and boundary elements (either linear or quadratic type).

The specifications of the computer codes used in this paper are as follows.

(1) Macro-elements were developed as an "ELMT04 subroutine" in the computer program MINIFEM that is cited in the book of Zienkiewicz [5]. In all cases a 2×2 Gaussian quadrature was applied on the $N_\xi \times N_\zeta$ internal cells within the patch, as those determined by the number of subdivisions of the sides $\xi = 0(N_\xi)$ and $\zeta = 0(N_\xi)$. It is remarkable that the structure of MINIFEM requires that the stiffness matrix is calculated *twice*: the first time to store the total matrix (macro-command: TANG) and the second time to calculate the right-hand side of equations (macro-command: FORM).

(2) Eigenvalue analysis was also performed using the above-mentioned code, which was properly enriched with the subspace-iteration subroutine that is cited in the book of Bathe [26].

(3) Boundary element analysis was performed by following the style of the codes cited in the book of Brebbia and Dominguez [15]. This means that the well-known **H** and **G** influence matrices were calculated *once* and boundary conditions were applied later. Eigenvalue BEM analysis was performed using the QR algorithm.

In many places below, the comparison is performed on the basis of the *mean average error* (in %) of the N involved values of a quantity x (appearing in the rows of the table under consideration), which is defined as follows:

$$\text{Error(in \%)} = \frac{1}{N}\sum_{i=1}^{N}\frac{|x_i - x_{i,\text{exact}}|}{|x_{i,\text{exact}}|} \times 100 \tag{14}$$

4.1. Test problem 1: steady-state conduction of a cylindrical wall

The first problem refers to the potential problem (1) with a "steep" temperature distribution, occurring essentially along the radius of the thick cylinder (Fig. 4a). The cylinder is subject to a uniform inner surface temperature at $T_i = 1000°C$ and a uniform external surface temperature of $T_e = 0°C$. The cylinder under consideration is assumed to be of infinite length. So, its upper and lower faces are insulated in order to prevent axial heat flow. According to Carslaw and Jaeger [28], at steady state the cylinder experiences the following temperature distribution in the radial direction:

$$T(r) = T_i + [(T_e - T_i)/\ln(R_e/R_i)]\ln(r/R_i) \tag{15}$$

where $R_i = 1$, $R_e = 32$ are the internal and external radii, respectively. Table 1 shows the results obtained using (i)

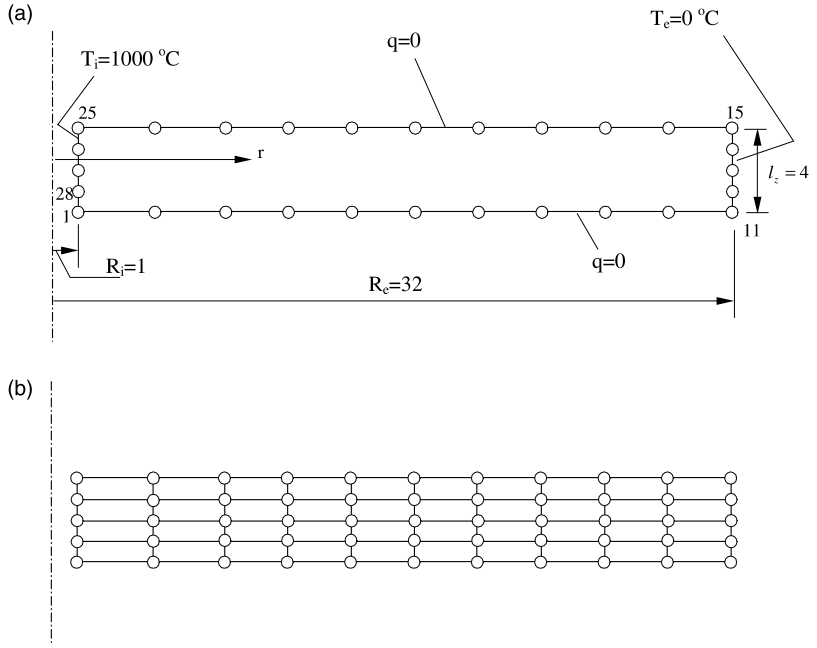

Fig. 4. Problem 1: steady-state conduction of a cylindrical wall: (a) geometry definition of a thick cylinder and macro-element discretization (28 DOF) and (b) finite element mesh (55 DOF).

Table 1
Problem 1: temperature distribution in a long cylinder with $R_e = 32$, $R_i = 1$ and radial heat flow

Radius (r)	Errors in %			Exact solution ($T(r)$)
	Macro-element	FEM	BEM	
1.00	Input	Input	Input	1000.000
4.10	+2.73	+5.56	−0.25	592.875
7.20	+3.89	+6.17	−0.51	430.400
10.30	+2.96	+6.36	−0.86	327.085
13.40	+3.52	+6.45	−1.15	251.167
16.50	+3.19	+6.50	−1.39	191.121
19.60	+3.39	+6.53	−1.59	141.443
22.70	+3.25	+6.56	−1.77	99.075
25.80	+3.38	+6.57	−1.95	62.140
28.90	+3.11	+8.28	−2.18	29.400
32.00	Input	Input	Input	0.000

Comparison of the 28-DOF macro-element with the FEM (55-DOF, 40 four-noded bilinear elements) and BEM (28 boundary elements of linear type).

a 28-DOF macro-element (ii) a 55-DOF finite element model and (iii) a 28-DOF boundary element model of linear interpolation. It should be also clarified that the origin of the four-sided Coons' patch was taken at the node "1", while the sides $\zeta = 0$ and $\xi = 1$ were consisted of the nodes "1–11" and "11–15", respectively. In this case, the opposite sides have the same number of segments ($N_\xi = 10$ and $N_\zeta = 4$).

Table 2
Problem 1: comparison between accuracy and efficiency in the three tested methods

Computational method	Mean average error (%)	CPU time (s)
FEM	6.55	0.06
Macro-element (proposed)	3.27	0.11
BEM	1.29	0.28

One can notice in Table 2 that the mean average error obtained by the proposed method is found between the conventional FEM and the BEM (for the same number of boundary nodes). It is also interesting that in all methods the required CPU time is proportional to the achieved accuracy. In fact, if one multiplies (in Table 2) the second with the third column, he/she will obtain similar figures. In other words, in this particular example whatever is gained in accuracy it is lost in computation time. Nevertheless, the previous comparison does not consider data preparation costs, which gives an advantage to the proposed macro-element method as also occurs in BEM.

Remark: Taking into consideration the specifications of the computer codes (as presented in the beginning of Section 4), it becomes evident that the efficiency of the proposed macro-element method will further increase when implemented in such a manner that to avoid calculating the stiffness matrix twice.

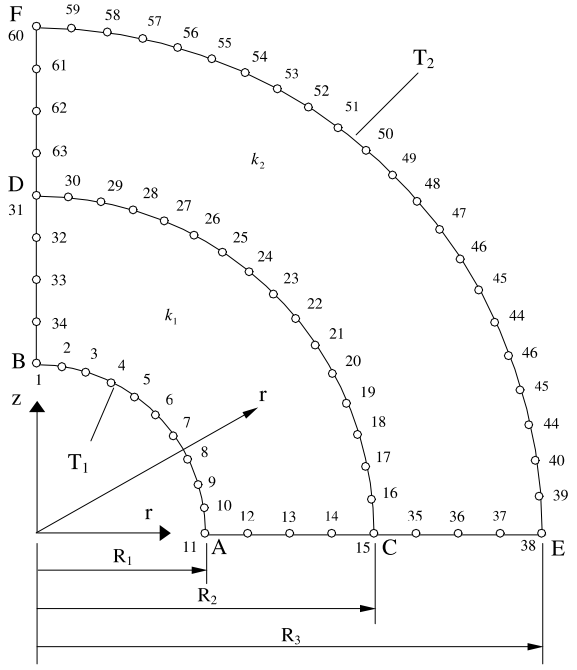

Fig. 5. Problem 2: macro-element mesh for compound sphere problem.

4.2. Test problem 2: compound sphere

Consider a compound sphere of two thick-walled spheres perfectly bonded to each other, with internal radius R_1, interface radius R_2 and external radius R_3 (Fig. 5). The inner surface of the inner sphere of conductivity k_1 is maintained at temperature T_1, while the outer surface of the outer sphere of conductivity k_2 is maintained at temperature T_2. The numerical values employed are $R_1 = 1.0$, $R_2 = 1.5$, $R_3 = 2.0$, $T_1 = 5.0$, $T_2 = 3.0$, $k_1 = 1.0$ and $k_2 = 2.0$. The analytical solutions for the temperatures and temperature gradients are given by Eqs. (16) and (17) (Carslaw and Jaeger [28]).

$$T = \frac{A}{r} + B \tag{16}$$

$$\frac{\mathrm{d}T}{\mathrm{d}n} = \frac{\mathrm{d}T}{\mathrm{d}r} = -\frac{A}{r^2} \tag{17}$$

For both spheres (1) and (2), the constants A and B are given by

$$A^{(1)} = \frac{R_1 R_2 (T_1 - T_c)}{R_2 - R_1}, \qquad A^{(2)} = \frac{R_2 R_3 (T_c - T_2)}{R_3 - R_2} \tag{18}$$

$$B^{(1)} = \frac{T_c R_2 - T_1 R_1}{R_2 - R_1}, \qquad B^{(2)} = \frac{T_2 R_3 - T_c R_2}{R_3 - R_2} \tag{19}$$

where T_c is the temperature along the common interface boundary, Γ_c.

By applying compatibility condition:

$$T^{(1)}(R_2) = T^{(2)}(R_2) \tag{20}$$

also the equilibrium condition:

$$k_1 \left[\frac{\mathrm{d}T}{\mathrm{d}n}\right]^{(1)}(R_2) = -k_2 \left[\frac{\mathrm{d}T}{\mathrm{d}n}\right]^{(2)}(R_2) \tag{21}$$

as well as, the prescribed temperatures at $r = R_1$ and R_3, a linear system of four equations and four unknowns is formulated. When solved, A and B are found 4.8 and 0.2 for the inner sphere and 2.4 and 1.8 for the outer sphere (Bakr [27]).

Due to the inhomogeneity, it is necessary to divide the problem domain in two separate areas, BACDB and DCEFD, which are occupied by two macro-elements, as shown in Fig. 5. Unlike the previous problem, in this case the opposite sides of each macro-element have different numbers of subdivisions N_ξ (AB: 10, CD: 16 and EF: 22 subdivisions). The calculated temperatures are very accurate and are shown in Table 3. With respect to the calculated fluxes along the common interface CD ($q = k_1 \partial T/\partial \mathbf{n} = k_2 \partial T/\partial \mathbf{n}$), these were found to be discontinuous (macro-element 1: $q = 2.2114$, macro-element 2: $q = 2.0420$) with mean average 2.1267 which differs only 0.3% than the exact value (2.1333). We recall that the discontinuity of the flux is consistent with the conventional finite elements, while in the BEM it holds per se.

Finally, it can be noticed at the bottom of Table 3 (bottom row) that in this case the proposed macro-elements are characterized by the same accuracy as the BEM using quadratic boundary elements. With respect to CPU time, the proposed method is more efficient than the BEM, as it requires only 0.72 s while BEM 0.99 s.

Table 3
Problem 2: temperature distribution in a compound sphere problem

Nodes	Radius	Temperature		
		Exact solution	Macro-element	BEM (quadratic type) [Ref. 27, p. 29]
1–11	1.0	5.0	Input	Input
12	1.125	4.4667	4.4648	4.4668
13	1.250	4.0400	4.0412	4.0403
14	1.375	3.6909	3.6895	3.6913
15–31	1.5	3.400	3.400[a]	3.3999
35	1.625	3.2769	3.2763	3.2770
36	1.75	3.1714	3.1715	3.1715
37	1.875	3.08	3.0797	3.0801
38–60	2.0	3.0	Input	Input
CPU time (s)			0.72	0.99[b]

[a] Values averaged over the nodes concerned.
[b] As implemented by the author of this paper.

Based on similar thoughts as those in the remark at the end of the test problem 1, it is obvious that the efficiency of the proposed method will further improve.

4.3. Test problem 3: cylindrical acoustical cavity

This third problem refers to the wave propagation (eigenvalues) in a cylindrical acoustical cavity of radius $r = 0.08$ m and length $l_z = 0.3$ m with Neumann boundary conditions ($\partial u/\partial \mathbf{n} = 0$) and velocity $c = 1$ m/s (Fig. 6). The exact eigenvalues are (Blevins [29]):

$$\omega_{p,q}^2 = \pi^2 c^2 \left[\left(\frac{p}{l_z^2} \right) + \left(\frac{\beta_q}{\pi r} \right)^2 \right] \tag{22}$$

where $p = 0, 1, 2, \ldots$ is an integer and β_q is the qth root of the Bessel function. For $q = 1$ it holds that the root $J_1(\beta_1) = 0$ is $\beta_1 = 3.8317$ (Morse and Feshbach [30, p. 1565]).

In this case, the macro-element approach with 32 DOFs is compared to the FEM using 48 four-noded bilinear elements with total 65 DOFs. In both cases, the number of the boundary DOFs is exactly the same. From Table 4 it can be noticed that the performance of the macro-element approach in this case is superior to that of the conventional FEM, although half of the DOFs are used. Specifically, as shown in the bottom row of Table 4, the mean average error is only 0.27% in contrast to 3.11%.

With respect to the required CPU time, the proposed method has the same efficiency as the conventional FEM (0.54 s versus 0.50 s). So, the overall behaviour of the proposed macro-element method is satisfactory.

Finally, the macro-element approach is compared with the dual reciprocity BEM (DR-BEM) using mass matrices proposed by Nardini and Brebbia [31] in conjunction with conical base functions ($f_j = R$) and boundary poles only. It was found that, for the same number of boundary nodes, DR-BEM (using linear type elements) is less efficient as it required 1.26 s. But although it has been previously reported that DR-BEM works satisfactory for elastodynamic problems [31], Table 4 depicts that when this technique is applied in axisymmetric acoustical cavities it does not behave well. It is reminded that this conclusion holds also for two-dimensional acoustical cavities and DR-BEM improves only when taking into consideration internal sources, as previously discussed in detail by the authors [32–34]. Of course, accurate BEM results can be alternatively obtained on the basis of Helmholtz equation using frequency-dependent fundamental solutions [35,36] but the resulting eigenvalue problem becomes nonalgebraic and, consequently, it requires still higher computer effort.

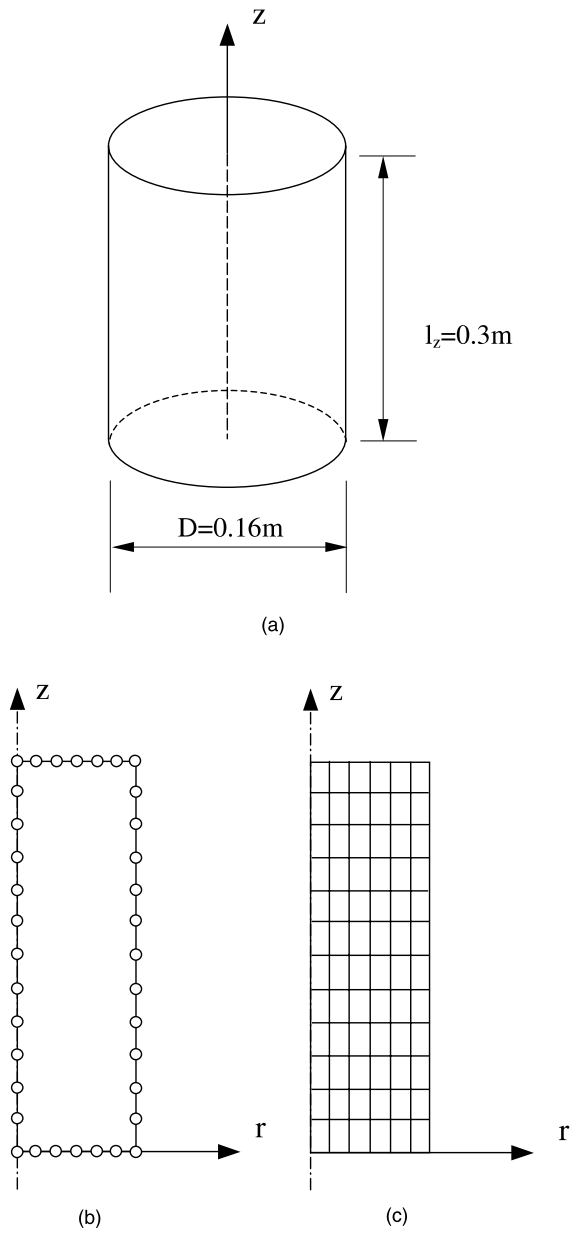

Fig. 6. Problem 3: cylindrical acoustical cavity: (a) general geometry and dimensions, (b) macro-element (36 DOF) and (c) conventional four-noded finite elements (91 DOF).

5. Conclusions and discussion

In this paper it was shown that macro-finite elements based on Coons' interpolation theory with B-splines interpolation of the boundary degrees of freedom are suitable for the solution of axisymmetric Laplace and eigenvalue wave propagation problems. The proposed

Table 4
Problem 3: eigenvalues of an axisymmetric acoustical cavity with $c = 1$ m/s, $r = 0.08$ m, $l_z = 0.3$ m and Neunmann boundary conditions

(p,q)	Errors in %			Exact solution (ω^2)
	Macro-element	FEM	BEM	
(0,0)	0.00	0.00	0.00	0.00
(1,0)	+0.03	+0.57	+4.12	109.66
(2,0)	+0.09	+2.30	+18.93	438.65
(3,0)	+0.20	+5.26	+31.44	986.72
(4,0)	+0.23	+9.43	+43.45	1754.59
(0,1)	+0.13	+2.16	+21.19	2294.06
(1,1)	+0.36	+2.09	+21.20	2403.73
(2,1)	+0.52	+2.18	+56.14	2732.71
(3,1)	−0.90	−3.99	+99.92	3281.03
Mean average error	0.27%	3.11%	37.05%	

Comparison of the 36-DOF macro-element with the FEM (91-DOF, 72 quadrilateral elements) and BEM (25-DOF, 24 elements of linear type).

macro-elements are applicable to arbitrary-shaped domains, and the degrees of freedom appear only at the boundaries of the entire field or along the boundaries of its subregions. The last are introduced when the domain is divided for the purpose of reducing the bandwidth or in order to deal with inhomogeneous problems characterized by different material properties. It should be clarified that in the case of a hollow structure, the discretization of the proposed macro-elements is very similar to that used in the BEM. However, in places where the structure is not hollow but it includes a part of the axis of symmetry, it is necessary to introduce nodal points along that, similarly to the case of the conventional finite elements. Finally, numerical results in two static problems and one eigenvalue problem have demonstrated the excellent performance of the proposed macro-element method.

Appendix A. Derivation of Coons' formula: geometry interpolation

Coons' interpolation formula refers to the geometry of a smooth curvilinear patch, which is mapped into a *reference square* surrounded by four sides AB, BC, CD and DA, as shown in Fig. 7a. It is assumed that along these four sides the boundary Cartesian coordinate vector $\mathbf{x}|_{\mathrm{AB,BC,CD,DA}} = \{x,z\}^{\mathrm{T}}$ is known. The objective is to interpolate the vector $\mathbf{x} = \{x,z\}^{\mathrm{T}}$ in the interior of the curvilinear patch for any given couple (ξ,ζ) of the normalized coordinates, which belong in the interval $[0,1] \times [0,1]$. A short description is given below.

When the vector $\mathbf{x}|_{\mathrm{AD}} = \{x,z\}^{\mathrm{T}}$ along the side AD ($\xi = 0$) is projected towards the opposite side BC ($\xi = 1$), using the blending function $E_0(\xi) = 1 - \xi$, the term $\mathbf{x}(0,\eta)E_0(\xi)$ is produced. Obviously, the last term presents accurately the side AD and has zero influence to the opposite side BC. By extending this concept to all four sides of the patch, the coordinate at an internal point (ξ,ζ) is a result of four relevant projections as follows:

$$\hat{\mathbf{x}}(\xi,\zeta) = E_0(\xi)\mathbf{x}(0,\zeta)|_{\mathrm{AD}} + E_1(\xi)\mathbf{x}(1,\zeta)|_{\mathrm{BC}} + E_0(\zeta)\mathbf{x}(\xi,0)|_{\mathrm{AB}} + E_1(\zeta)\mathbf{x}(\xi,1)|_{\mathrm{CD}} \tag{A.1}$$

However, when Eq. (A.1) is applied along the side AB ($\zeta = 0$) it leads to

$$\hat{\mathbf{x}}(\xi,0) = \mathbf{x}(\xi,0) + E_0(\xi)\mathbf{x}(0,0) + E_1(\xi)\mathbf{x}(1,0) \tag{A.2}$$

In other words, Eq. (A.2) denotes that it is necessary to subtract the "correcting" term

$$\mathrm{CT}_{\mathrm{AB}} = E_0(\xi)\mathbf{x}(0,0) + E_1(\xi)\mathbf{x}(1,0), \quad \zeta = 0 \tag{A.3}$$

from $\hat{\mathbf{x}}(\xi,\zeta)$ (Eq. (A.1)), so as the boundary AB is accurately represented. This correcting term consists of the nodal coordinates at the edges of the side AB, multiplied by blending functions of which the index corresponds to the natural ξ-coordinate of each edge.

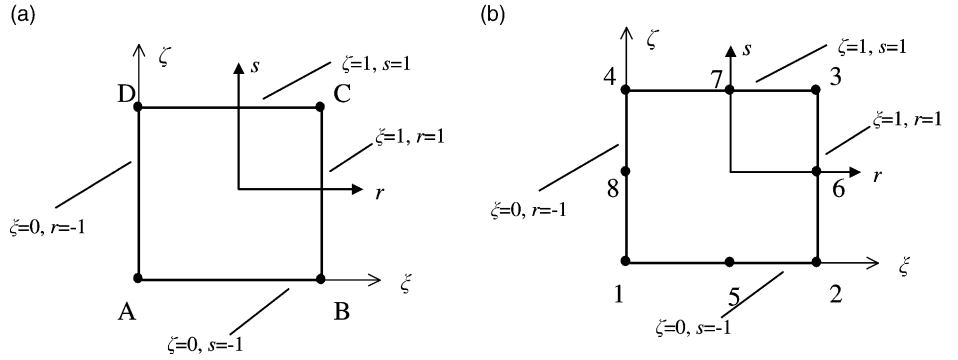

Fig. 7. Reference square for (a) bilinear element and (b) quadratic element.

In a similar way, for the rest three sides the correcting terms are given as:

$$\text{side BC} \quad \mathrm{CT}_{\mathrm{BC}} = E_0(\eta)\mathbf{x}(1,0) + E_1(\eta)\mathbf{x}(1,1), \quad \xi = 1 \tag{A.4}$$

$$\text{side CD} \quad \mathrm{CT}_{\mathrm{CD}} = E_0(\xi)\mathbf{x}(0,1) + E_1(\xi)\mathbf{x}(1,1), \quad \zeta = 1 \tag{A.5}$$

$$\text{side AD} \quad \mathrm{CT}_{\mathrm{AD}} = E_0(\eta)\mathbf{x}(0,0) + E_1(\eta)\mathbf{x}(0,1), \quad \xi = 0 \tag{A.6}$$

A careful inspection of Eqs. (A.3)–(A.6) reveals that each edge is influenced by two blending functions in both directions. For example, $\mathbf{x}(0,0)$ is multiplied by both functions $E_0(\xi)$ (Eq. (A.3)) and $E_0(\zeta)$ (Eq. (A.6)). Since the blending functions

$$\begin{aligned} &E_0(\xi) = 1-\xi, \qquad E_1(\xi) = \xi, \\ &E_0(\zeta) = 1-\zeta, \qquad E_1(\zeta) = \zeta \end{aligned} \tag{A.7}$$

are characterized by cardinality, that is

$$E_i(\xi_j) = \delta_{ij} \tag{A.8}$$

it is trivial to conclude that for any point along the boundary (AB, AD) the correcting term that corresponds to the edge A is given as $\mathbf{x}(0,0)E_0(\xi)E_0(\zeta)$.

By extending the above concept, for any arbitrary point (ξ,ζ) inside the patch the final correcting term becomes

$$\mathrm{CT} = \sum_{i=0}^{1}\sum_{j=0}^{1}\mathbf{x}(i,j)E_i(\xi)E_j(\zeta) \tag{A.9}$$

when CT is subtracted from Eq. (A.1) one receives

$$\mathbf{x}(\xi,\zeta) = \hat{\mathbf{x}}(\xi,\zeta) - \mathrm{CT} \tag{A.10}$$

and, therefore, the final interpolation formula becomes:

$$\begin{aligned} \mathbf{x}(\xi,\zeta) = {} & E_0(\xi)\mathbf{x}(0,\zeta) + E_1(\xi)\mathbf{x}(1,\zeta) + E_0(\zeta)\mathbf{x}(\xi,0) \\ & + E_1(\zeta)\mathbf{x}(\xi,1) - E_0(\xi)E_0(\zeta)\mathbf{x}(0,0) \\ & - E_1(\xi)E_0(\zeta)\mathbf{x}(1,0) - E_0(\xi)E_1(\zeta)\mathbf{x}(0,1) \\ & - E_1(\xi)E_1(\zeta)\mathbf{x}(1,1) \end{aligned} \tag{A.11}$$

For further details the interested reader may consult classical textbooks [37,38].

Appendix B. Construction of global shape functions using Coons' interpolation

The key ingredient to develop global shape functions is to apply the idea of *isoparametric* element by extending Eq. (A.11) from geometry to the potential interpolation as follows:

$$\begin{aligned} u(\xi,\zeta) = {} & E_0(\xi)u(0,\zeta) + E_1(\xi)u(1,\zeta) \\ & + E_0(\zeta)u(\xi,0) + E_1(\zeta)u(\xi,1) \\ & - E_0(\xi)E_0(\zeta)u(0,0) - E_1(\xi)E_0(\zeta)u(1,0) \\ & - E_0(\xi)E_1(\zeta)u(0,1) - E_1(\xi)E_1(\zeta)u(1,1) \end{aligned} \tag{B.1}$$

The construction of the Coons-based global shape functions is introduced through two trivial examples (four- and eight-node elements). The extension of the method to larger elements with more nodes is straightforward.

B.1. Example 1: bilinear elements

Let us here assume that the potential u along the four sides (Fig. 7a) is linearly interpolated as follows $(0 \leqslant \xi,\zeta \leqslant 1)$:

$$\begin{aligned} &u_{\mathrm{AD}} \equiv u(0,\zeta) = (1-\zeta)u_{\mathrm{A}} + \zeta u_{\mathrm{D}} \\ &u_{\mathrm{BC}} \equiv u(1,\zeta) = (1-\zeta)u_{\mathrm{B}} + \zeta u_{\mathrm{C}} \\ &u_{\mathrm{AB}} \equiv u(\xi,0) = (1-\xi)u_{\mathrm{A}} + \xi u_{\mathrm{B}} \\ &u_{\mathrm{CD}} \equiv u(\xi,1) = (1-\xi)u_{\mathrm{D}} + \xi u_{\mathrm{C}} \end{aligned} \tag{B.2}$$

By substituting Eq. (B.2) in Eq. (B.1) and then eliminating the opposite terms, one finally receives

$$\begin{aligned} u(\xi,\zeta) = {} & u_{\mathrm{A}}(1-\xi)(1-\zeta) + u_{\mathrm{B}}\xi(1-\zeta) \\ & + u_{\mathrm{C}}\xi\zeta + u_{\mathrm{D}}(1-\xi)\zeta \end{aligned} \tag{B.3}$$

Remark. Using now the well-known natural coordinates $(-1 \leqslant r,s \leqslant +1)$:

$$r = 2\xi - 1, \qquad s = 2\zeta - 1 \tag{B.4}$$

and substituting in Eq. (B.3), one receives

$$\begin{aligned} u = {} & u(r,s) \\ = {} & u_{\mathrm{A}}\frac{(1-r)(1-s)}{4} + u_{\mathrm{B}}\frac{(1+r)(1-s)}{4} \\ & + u_{\mathrm{C}}\frac{(1+r)(1+s)}{4} + u_{\mathrm{D}}\frac{(1-r)(1+s)}{4} \end{aligned} \tag{B.5}$$

Eq. (B.5) is the well-known expression for bilinear finite elements [26].

B.2. Example 2: quadratic eight-node elements

Let us here assume that the potential u along each of the four sides of the patch (Fig. 7b) is interpolated through a polynomial of second degree. So, for the three nodes $(\zeta = 0, 1/2, 1)$ along the boundary side of the patch with $\xi = 0$ or 1, we define the corresponding Lagrange polynomials as follows $(0 \leqslant \xi,\zeta \leqslant 1)$:

$$\begin{aligned} &L_0(\zeta) = 1 - 3\zeta + 2\zeta^2, \\ &L_{1/2}(\zeta) = 4(\zeta - \zeta^2), \qquad L_1(\zeta) = -\zeta + 2\zeta^2 \end{aligned} \tag{B.6}$$

Similar polynomials can be defined for the rest two sides ($\zeta = 0$ or 1). By interpolating the potential along each side using the previously mentioned Lagrange polynomials and then substituting in Eq. (B.1), one obtains:

$$\begin{aligned} u(\xi,\zeta) = {} & E_0(\xi)\left[L_0(\zeta)u_1 + L_{1/2}(\zeta)u_8 + L_1(\zeta)u_4\right] \\ & + E_1(\xi)\left[L_0(\zeta)u_2 + L_{1/2}(\zeta)u_6 + L_1(\zeta)u_3\right] \\ & + E_0(\zeta)\left[L_0(\xi)u_1 + L_{1/2}(\xi)u_5 + L_1(\xi)u_2\right] \\ & + E_1(\zeta)\left[L_0(\xi)u_4 + L_{1/2}(\xi)u_7 + L_1(\xi)u_3\right] \\ & - E_0(\xi)E_0(\zeta)u_1 - E_1(\xi)E_0(\zeta)u_2 \\ & - E_0(\xi)E_1(\zeta)u_4 - E_1(\xi)E_1(\zeta)u_3 \end{aligned} \tag{B.7}$$

and after re-arranging the terms:

$$\begin{aligned} u(\xi,\zeta) = {} & u_1[E_0(\xi)L_0(\zeta) + L_0(\xi)E_0(\zeta) - E_0(\xi)E_0(\zeta)] \\ & + u_2[E_1(\xi)L_0(\zeta) + L_1(\xi)E_0(\zeta) - E_1(\xi)E_0(\zeta)] \\ & + u_3[E_1(\xi)L_1(\zeta) + L_1(\xi)E_1(\zeta) - E_1(\xi)E_1(\zeta)] \\ & + u_4[E_0(\xi)L_1(\zeta) + L_0(\xi)E_1(\zeta) - E_0(\xi)E_1(\zeta)] \\ & + u_5\left[L_{1/2}(\xi)E_0(\zeta)\right] + u_6\left[E_1(\xi)L_{1/2}(\zeta)\right] \\ & + u_7\left[L_{1/2}(\xi)E_0(\zeta)\right] + u_8\left[E_0(\xi)L_{1/2}(\zeta)\right] \end{aligned} \tag{B.8}$$

Obviously, the functions being into the brackets $[\cdots]$ of Eq. (B.8) correspond to the shape functions $N_j(\xi,\zeta)$ for the degrees of freedom $u_1,\ldots,u_8$.

Remark. By combining Eqs. (A.7), (B.4) and (B.6) and substituting into Eq. (B.8), it can be easily found that the shape functions appeared in Eq. (B.8) are identical with those of the classical Serendipity eight-node isoparametric element, i.e.:

Corner nodes (1, 2, 3 *and* 4):

$$N_i = \tfrac{1}{4}(1+\xi_0)(1+\zeta_0)(\xi_0+\zeta_0-1)$$

Mid-side nodes (5, 6, 7 *and* 8):

$$\xi_i = 0, \quad N_i = \tfrac{1}{2}(1-\xi^2)(1+\zeta_0)$$
$$\zeta_i = 0, \quad N_i = \tfrac{1}{2}(1+\xi_0)(1-\zeta^2)$$
$$\xi_0 = \xi\xi_i, \quad \zeta_0 = \zeta\zeta_i$$

References

[1] Ritz W. Über eine neue Methode zur Lösung gewisser Variationsprobleme der mathematischen Physik. Zeitschrift für Angewandte Mathematik und Mechanik 1908; 135(1):1–61.

[2] Finlayson BA. The method of weighted residuals. New York: Academic Press; 1972.

[3] Trefftz E. Ein Gegenstück zum Ritz'schen Verfahren. Proceedings, Second International Congress in Applied Mechanics, Zurich, 1926.

[4] Argyris JH, Kelsey S. Energy theorems and structural analysis. Aircraft Engng 1955:26-27.

[5] Zienkiewicz OC. The finite element method. 3rd ed. London: McGraw-Hill; 1977.

[6] Irons BM. Engineering application of numerical integration in stiffness method. AIAA J 1966;14(11):2035–7.

[7] Coons SA. Surfaces for computer aided design of space form, Project MAC, MIT (1964), revised for MAC-TR-41. Springfield, VA, USA: Available by CFSTI, Sills Building, 5285 Port Royal Road, 1967.

[8] Gordon WJ. Blending functions methods of bivariate multivariate interpolation and approximation. SIAM J Numer Anal 1971;8:158–77.

[9] Gordon WJ, Hall CA. Transfinite element methods blending function interpolation over arbitrary curved element domains. Numer Math 1973;21:109–12.

[10] Zafrany El, Cookson RA. Derivation of Lagrangian and Hermiatian shape functions for quadrilateral elements. Int J Numer Meth Engng 1986;23:1939–58.

[11] Jirousek J, Leon N. A powerful finite element for plate bending. Comput Meth Engng 1977;24:77–96.

[12] Jirousek J. Basis for development of large elements locally satisfying all field equations. Comput Meth Appl Mech Engng 1978;14:65–92.

[13] Jirousek J, Theodorescu P. Large finite elements method for the solution of problems in the theory of elasticity. Comput Struct 1982;15(5):575–87.

[14] Jirousek J, Guex L. The hybrid-Trefftz finite element model and its application to plate blending. Int J Numer Meth Engng 1986;23:651–93.

[15] Brebbia CA, Dominguez J. Boundary elements: an introductory course. Southampton: Computational Mechanics Publications, McGraw-Hill Book Company; 1992.

[16] Kanarachos A, Grekas D, Provatidis Ch. Generalized formulation of Coons's interpolation. In: Kaklis PD, Sapidis NS, editors. Computer aided geometric design: from theory to practice. Athens: National Technical University of Athens Press; 1995. p. 65–76 [Chapter 7].

[17] Röper O. Ein Geometrieprozessor für die rechnerunterstützte Auslegung von Maschinenbauteilen mit Hilfe der Methode der Finite Elemente. Dissertation. Ruhr-Universität Bochum, 1978.

[18] Kanarachos A, Röper O. Rechnerunterstützte Netzgeneriegung mit Hilfe der Coonsschen Abbildung, VDI-Z 1979;121:297–303.

[19] Yildir YB, Wexler A. MANDAP – A FEM/BEM preparation package. IEEE Trans Magnetics 1983;19:2562–5.

[20] Barnhill RE, Gregory JA. Compatible smooth interpolation on triangles. J Approx Theory 1975;15:214–25.

[21] Barhill E, Mansfield L. Error bounds for smooth interpolation on triangles. J Approx Theory 1974;11:306–18.

[22] Barhill E, Birkhoff E, Gordon MJ. Smooth interpolation on triangles. J Approx Theory 1973;8:114–28.

[23] Zhaobei X, Zhiqiang. Coons' surface method for formulation of finite element of plate and shells. Comput Struct 1987;27:79–88.

[24] Kanarachos A, Deriziotis D. On the solution of Laplace and wave propagation problems using C-elements. Finite Element Anal Des 1989;5:97–109.

[25] Kanarachos A, Provatidis Ch, Deriziotis DG, Foteas N. A new approach of the FEM analysis of two-dimensional

elastic structures using global (Coons's) interpolation functions. In: Wunderlich J, editor. CD Proceedings, European Conference on Computational Mechanics. München, Germany, 1999.
[26] Bathe KJ. Finite element procedures in engineering analysis. New Jersey: Prentice-Hall; 1982.
[27] Bakr A. The Boundary integral equation method in axisymmetric stress analysis problems. Lecture Notes in Engineering, vol. 14. Berlin: Springer; 1986.
[28] Carslaw HS, Jaeger JC. Conduction of heat in solids. London: Oxford University Press; 1959.
[29] Blevins RD. Formulas for natural frequency and mode shape. New York: Van Nostrand; 1979.
[30] Morse PM, Feshbach H. Methods of theoretical physics. New York: McGraw-Hill; 1953.
[31] Nardini D, Brebbia CA. Boundary integral formulation of mass matrices for dynamic analysis. In: Brebbia CA, editor. Topics in boundary element research-2. Berlin: Springer; 1985, p. 152–69.
[32] Provatidis Ch. Application of the boundary element method in the analysis of field and dynamic problems. Doctoral Dissertation, National Technical University of Athens, 1987.
[33] Kanarachos A, Provatidis Ch. Performance of mass matrices for the BEM dynamic analysis of wave propagation problems. Comput Meth Appl Mech Engng 1987;63: 155–65.
[34] Provatidis Ch, Kanarachos A. Further research on the performance of consistent mass matrices using BEM for symmetric/nonsymmetric formulations. Comput Mech 1995; 16:197–207.
[35] Tai G, Shaw RP. Helmholtz equation eigenvalues and eigenmodes for arbitrary domains. J Acoust Soc Amer 1974;56:796–804.
[36] Mey De. Calculation of eigenvalues of the Helmholtz equation by an integral equation. Int J Numer Meth Engng 1976;10:59–66.
[37] Faux ID, Pratt MJ. Computational geometry for design and manufacture. Chichester: Ellis Horwood; 1979.
[38] Farin G. Curves and surfaces for computer aided geometric design: a practical guide. Boston: Academic Press; 1990.